

Discovery of N-{4-[(6,7-dimethoxyquinazolin-4-yl)oxy]phenyl}-2-[4-(propan-2-yl)-1H-1,2,3-triazol-1-yl]acetamide (AZD3229), a potent pan-KIT mutant inhibitor for the treatment of gastrointestinal stromal tumors

Jason Grant Kettle, Rana Anjum, Evan Barry, Deepa Bhavsar, Crystal Brown, Scott Boyd, Andrew Campbell, Kristin Goldberg, Michael Grondine, Sylvie Guichard, Christopher Hardy, Tom Hunt, Rhys Jones, Xiuwei Li, Olga Moleva, Derek Ogg, Ross Overman, Martin J Packer, Stuart Pearson, Marianne Schimpl, Wenlin Shao, Aaron Smith, James Smith, Darren Stead, Stephen Stokes, Michael Tucker, and Yang Ye

J. Med. Chem., **Just Accepted Manuscript** • DOI: 10.1021/acs.jmedchem.8b00938 • Publication Date (Web): 11 Sep 2018

Downloaded from <http://pubs.acs.org> on September 11, 2018

Just Accepted

“Just Accepted” manuscripts have been peer-reviewed and accepted for publication. They are posted online prior to technical editing, formatting for publication and author proofing. The American Chemical Society provides “Just Accepted” as a service to the research community to expedite the dissemination of scientific material as soon as possible after acceptance. “Just Accepted” manuscripts appear in full in PDF format accompanied by an HTML abstract. “Just Accepted” manuscripts have been fully peer reviewed, but should not be considered the official version of record. They are citable by the Digital Object Identifier (DOI®). “Just Accepted” is an optional service offered to authors. Therefore, the “Just Accepted” Web site may not include all articles that will be published in the journal. After a manuscript is technically edited and formatted, it will be removed from the “Just Accepted” Web site and published as an ASAP article. Note that technical editing may introduce minor changes to the manuscript text and/or graphics which could affect content, and all legal disclaimers and ethical guidelines that apply to the journal pertain. ACS cannot be held responsible for errors or consequences arising from the use of information contained in these “Just Accepted” manuscripts.

1
2
3 **Discovery of *N*-{4-[(6,7-dimethoxyquinazolin-4-yl)oxy]phenyl}-2-[4-**
4 **(propan-2-yl)-1*H*-1,2,3-triazol-1-yl]acetamide (AZD3229), a potent pan-**
5 **KIT mutant inhibitor for the treatment of gastrointestinal stromal tumors**
6
7
8
9

10
11
12
13 Jason G. Kettle,^{*†} Rana Anjum,[§] Evan Barry,^{§1} Deepa Bhavsar,[§] Crystal Brown,[§] Scott
14 Boyd,[†] Andrew Campbell,[†] Kristin Goldberg,[†] Michael Grondine,[§] Sylvie Guichard,^{§2}
15 Christopher J. Hardy,[¶] Tom Hunt,[†] Rhys D.O. Jones,[†] Xiuwei Li,[¥] Olga Moleva,[†] Derek
16 Ogg,^{¶3} Ross C. Overman,[¶] Martin J. Packer,[†] Stuart Pearson,[†] Marianne Schimpl,[¶] Wenlin
17 Shao,[§] Aaron Smith,[†] James M. Smith,[†] Darren Stead,[†] Steve Stokes,[†] Michael Tucker,[†] Yang
18 Ye[¥]
19
20
21
22
23
24
25
26
27
28
29

30 [†]Oncology, IMED Biotech Unit, AstraZeneca, Unit 310 - Darwin Building, Cambridge
31 Science Park, Milton Road, Cambridge, CB4 0WG, United Kingdom.
32
33

34 [¶]Discovery Sciences, IMED Biotech Unit, AstraZeneca, Unit 310 - Darwin Building,
35 Cambridge Science Park, Milton Road, Cambridge, CB4 0WG, United Kingdom.
36
37
38
39

40 [§]Oncology, IMED Biotech Unit, AstraZeneca, 35 Gatehouse Park, Waltham MA 02451,
41 USA.
42
43
44

45 [¥]Pharmaron Beijing Co., Ltd. 6 Taihe Road BDA, Beijing 100176 P. R. China
46
47
48
49

50
51 ¹ Current address: H3 Biomedicine Inc. 3520, 300 Technology Square floor 5, Cambridge, MA 02139, USA.

52 ² Current address: Forma Therapeutics Inc. Forma Therapeutics, 500 Arsenal St, Watertown, MA 02472, USA.

53 ³ Current address: Peak Proteins Ltd., 3G48 Mereside, Alderley Park, Macclesfield, Cheshire, SK10 4TG, UK.
54
55
56
57
58
59
60

1
2
3 **Abstract** While the treatment of Gastrointestinal Stromal Tumors (GIST) has been
4 revolutionised by the application of targeted tyrosine kinase inhibitors capable of inhibiting
5 KIT-driven proliferation, diverse mutations to this kinase drive resistance to established
6 therapies. Here we describe the identification of potent pan-KIT mutant kinase inhibitors that
7 can be dosed without being limited by the tolerability issues seen with multi-targeted agents.
8 This effort focussed on identification and optimisation of an existing kinase scaffold through
9 the use of structure-based design. Starting from a series of previously reported
10 phenoxyquinazoline and quinoline based inhibitors of the tyrosine kinase PDGFR α , potency
11 against a diverse panel of mutant KIT driven Ba/F3 cell lines was optimised, with a particular
12 focus on reducing activity against a KDR driven cell model in order to limit the potential for
13 hypertension commonly seen in second and third line GIST therapies. AZD3229
14 demonstrates potent single digit nM growth inhibition across a broad cell panel, with good
15 margin to KDR-driven effects. Selectivity over KDR can be rationalised predominantly by
16 the interaction of water molecules with the protein and ligand in the active site and its kinome
17 selectivity is similar to the best of the approved GIST agents. This compound demonstrates
18 excellent cross-species pharmacokinetics, shows strong pharmacodynamic inhibition of
19 target, and is active in several in vivo models of GIST.
20
21
22
23
24
25
26
27
28
29
30
31
32
33
34
35
36
37
38
39
40
41
42

43 **Introduction** Gastrointestinal Stromal Tumors (GIST) are soft tissue sarcomas of the
44 gastrointestinal (GI) tract that are driven predominantly through aberrant signalling of the
45 proto-oncogene c-KIT.¹ Following surgical resection, five-year survival rates vary from 35 -
46 65% depending on the size of tumor, mitotic potential, and where it is located.² Whilst
47 incidence is relatively rare, estimated to be of the order of 1.5 patients per 100,000 population
48 annually³ (annual incidence in the United States is estimated at 3800),⁴ GIST is still the most
49 common mesenchymal tumor of the GI tract, with the majority harbouring activating
50
51
52
53
54
55
56
57
58
59
60

1
2
3 mutations of this receptor tyrosine kinase.⁵ Such mutations are diverse and heterogeneous,
4
5 spanning the kinase domain of KIT with single point amino acid transpositions in the ATP
6
7 binding pocket, sequence deletions in exon 11, insertions in exon 9, with concurrent primary
8
9 and secondary mutational sites being common. A smaller subset of GIST tumors are instead
10
11 driven by mutations in the related tyrosine kinase, platelet-derived growth factor receptor- α
12
13 (PDGFR α). The D842V mutant of PDGFR α in particular, is equivalent to the KIT D816X
14
15 mutations, which are refractory to current therapies.⁶
16
17
18
19
20

21
22 Beyond surgical removal, treatment of GIST has been revolutionised by the application of
23
24 targeted tyrosine kinase inhibitors capable of inhibiting KIT-driven proliferation. Imatinib **1**,
25
26 an inhibitor of both c-KIT and PDGFR α , was initially approved in 2002 and granted
27
28 accelerated approval in 2008 as first line adjuvant treatment following surgery.⁷ Clinical trials
29
30 have demonstrated a 5-year overall survival rate of 92% following 3-year therapy, compared
31
32 with 82% for those taking the drug for one year. However, up to 20% of GIST patients
33
34 exhibit primary resistance to imatinib, and many patients taking imatinib will eventually
35
36 relapse due to secondary mutations which are unresponsive to therapy, although in some case
37
38 higher doses of the drug may prove effective.⁸ In 2006, the FDA approved multi-targeted
39
40 kinase inhibitor sunitinib **2** as a second line treatment for GIST patients who are refractory to,
41
42 or intolerant of imatinib therapy. In these patients, time-to-tumor progression of sunitinib-
43
44 treated patients was superior to that of placebo-treated patients.⁹ A second multi-targeted
45
46 kinase inhibitor, regorafenib **3**, was approved as third line therapy in 2013 for patients with
47
48 GIST that is not amenable to surgery and is refractory to both imatinib and sunitinib.
49
50 Approval was again based upon improved progression free survival (PFS) versus placebo.¹⁰
51
52
53
54 Despite the availability of these targeted agents, many clinically observed mutants of c-KIT
55
56 remain unresponsive, and there remains a significant unmet need in this disease for agents
57
58
59
60

with a much broader mutant KIT inhibition profile. The tolerability of sunitinib and regorafenib therapy, whilst clinically manageable, may also present challenges.¹¹ Toxicities associated with their multi-targeted kinase inhibition profile can lead to dose reductions and drug holidays, which may in theory exacerbate emergence of further resistant clones. Potent inhibition of VEGFR in these agents is associated with significant high-grade hypertension, amongst other significant toxicities.¹²

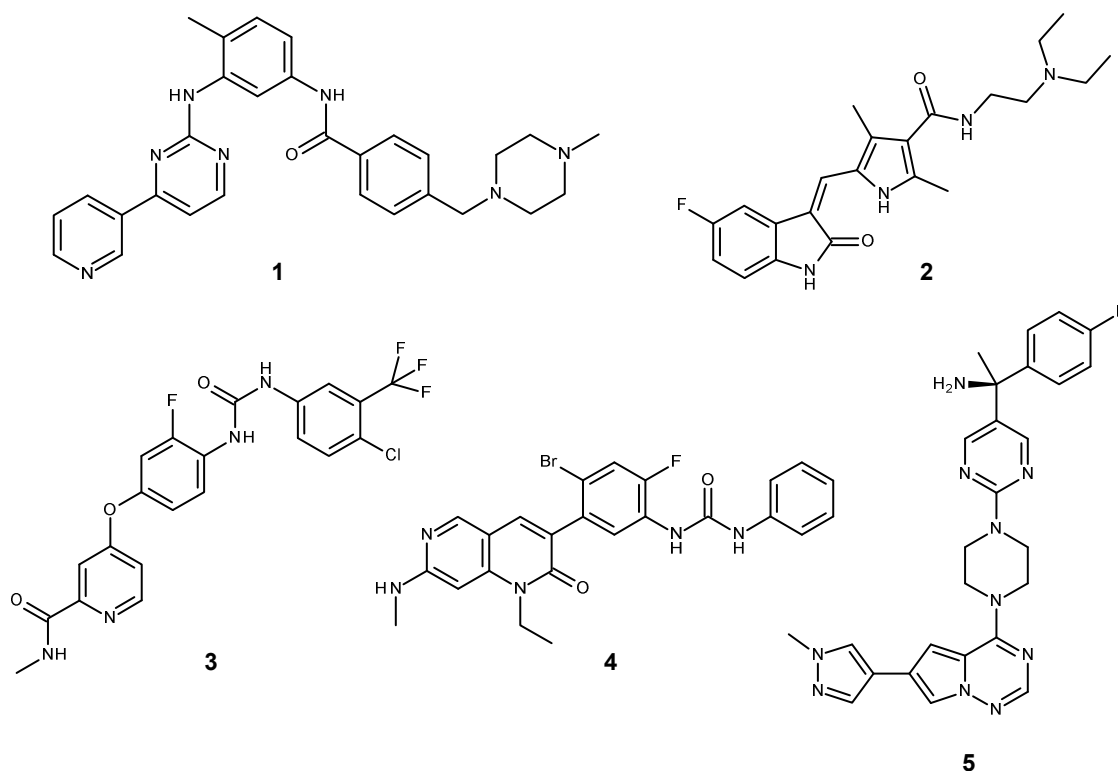
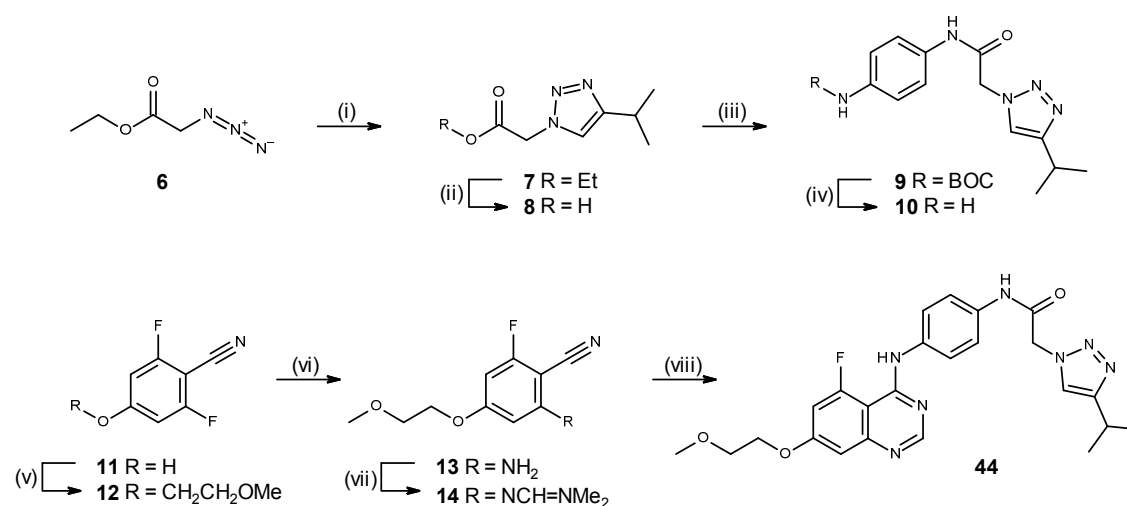


Figure 1. Approved GIST therapies and agents in clinical trials. Imatinib **1**, sunitinib **2**, regorafenib **3** are approved as first, second and third line treatments respectively. Ripretinib (DCC-2618) **4** and avapritinib (BLU-285) **5** are currently undergoing clinical trials in GIST patients.

Chemistry The synthesis of inhibitors **15** and **16** (Table 2) and related analogues **17** – **21** (Table 3) have been previously described.^{13, 14, 15, 16} A representative synthesis of compound **44** is shown in Scheme 1, with detailed experimental conditions for additional compounds available as Supplementary Information. Accordingly, copper-catalysed cycloaddition of ethyl azido acetate **6** with 3-methylbut-1-yne gives triazole **7** which was hydrolysed to

1
2
3 carboxylic acid **8**. Amide coupling of **8** with a BOC-protected *bis*-aniline gave **9** and removal
4 of the protecting group afforded aniline **10**. Starting from difluorocyanophenol **11**, alkylation
5 gave methoxyethyl ether **12**, and displacement of one fluoro atom with ammonia under
6 microwave heating gave aniline **13**. This was converted to the dimethylformimidamide
7 cyclisation precursor **14** and condensation of this with prepared aniline **10** in acetic acid gave
8
9
10
11
12
13
14
15
16
17
18
19
20
21
22
23
24
25
26
27
28
29
30
31
32
33
34
35
36
37
38
39
40
41
42
43
44
45
46
47
48
49
50
51
52
53
54
55
56
57
58
59
60

Scheme 1. Synthesis of compound **44**.



Reagents and conditions: (i) CuI, 3-methylbut-1-yne, Et₃N, CH₃CN, 20°C, 3 days, 90%; (ii) LiOH, water, THF, 20°C, 1.5 h, 100%; (iii) *tert*-Butyl *N*-(4-aminophenyl)carbamate, HATU, DIPEA, DMF, 20°C, 16 h, 57%; (iv) 4M HCl in dioxane, MeOH, DCM, 20°C, 3 h, 89%; (v) 1-Bromo-2-methoxyethane, K₂CO₃, DMF, 85°C, 5 h, 93%; (vi) aq. NH₃, *i*-PrOH, 100°C, 13 h, 87%; (vii) 1,1-Dimethoxy-*N,N*-dimethylmethanamine, 80°C, 2 h, 100%; (viii) **10**, acetic acid, 60°C, 35 mins, 58%.

Results and discussion In order to screen for broad spectrum mutant c-KIT inhibitors with low potential for hypertension, we established a panel of Ba/F3 cell lines expressing a variety

1
2
3 of clinically relevant secondary mutants of c-KIT, spanning the ATP binding sequence
4 (V654A, T670I gatekeeper) and the A-loop (D816H, D820A, D823Y and others) all on a
5 background of a primary exon 11 deletion (of amino acids 557 and 558), together with a line
6 expressing Tel-KDR to monitor selectivity over KDR (VEGFR2). In this latter line, KDR is
7 expressed as a fusion protein with a Tel sequence at the *N*-terminus, resulting in constitutive
8 kinase activity. We chose exon 11 deletion as the primary mutation and the backbone for all
9 the secondary mutations since two-thirds of GIST tumors harbor mutations in exon 11. Exon
10 11 deletions are associated with a shorter progression-free and overall survival in comparison
11 to the other exon 11 mutations. In particular, deletions involving codon 557 and/or codon 558
12 are associated with malignant behaviour.^{17,18} Proliferation of these cell lines is dependent
13 upon the introduced construct for growth, and so to monitor for non-specific effects on
14 viability in these cells, a parental Ba/F3 line (no introduced construct) is run in parallel.
15 Engineered cell lines including Ba/F3 have been shown previously to faithfully mimic
16 clinical efficacy of various agents in GIST.^{19,20} It is notable that all approved therapies are
17 type II kinase inhibitors, binding to the DFG-out kinase form, and in particular, c-KIT is one
18 of only a small number of kinases that prefers to exist in the DFG out form in its ground
19 state.²¹ Additionally c-KIT has an unusual activation profile in that the activation loop seems
20 not to require presence of phosphate²² and as type II inhibition in general is difficult to
21 reproduce in biochemical assays, given reliance on the activation state, we viewed a cellular
22 cascade as preferred for hit finding activities. Profiling of the various approved therapies in
23 these lines is informative (Table 1). In line with clinical experience, **1** shows only modest
24 activity against exon 11 deletion + V654A and D816H, and no activity at all against the
25 gatekeeper T670I mutation. Sunitinib **2** is potent against V654A and T670I, but has weak
26 activity against D816H. Regorafenib **3** is potent against the T670I mutant but is rather
27 modest against the others, and both **2** and **3** show potent inhibition of the Tel-KDR line
28
29
30
31
32
33
34
35
36
37
38
39
40
41
42
43
44
45
46
47
48
49
50
51
52
53
54
55
56
57
58
59
60

consistent with their potent effect on VEGFR2. Beyond these approved agents, additional compounds are currently undergoing clinical trials in GIST patients, aimed at targeting mutants of KIT not currently addressed in the clinic, with secondary D816H being a particularly refractory example. Ripretinib (DCC-2618), **4** is a potent pan-KIT and PDGFR inhibitor from Deciphera Pharmaceuticals and shows broad inhibition across this mutant panel.²³ It is also a potent inhibitor of the Tel-KDR line however and indeed grade 3/4 hypertension has been reported in a recent phase 1 clinical study of this compound.²⁴ Avapritinib (BLU-285), **5** from Blueprint Medicines is a potent inhibitor of KIT exon 17 mutations including D816 variants and also PDGFR.²⁵ In this panel it potently inhibits exon 11 deletion + D816H although is weaker against V654A and T670I. It has good selectivity for Tel-KDR, but a moderate signal in the parental line may reflect other kinase activities for this agent.

Table 1. Growth inhibition potency of GIST treatments in KIT mutant Ba/F3 lines and effect on Tel-KDR.

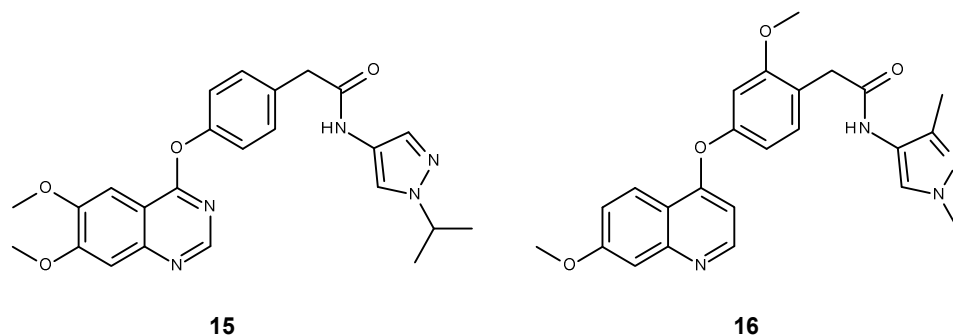
ID	Phase	Ba/F3 GI ₅₀ (μM)				KDR
		Parental	exon 11 del + V654A	exon 11 del +D816H	exon 11 del + T670I	
1 Imatinib	Approved 1 st line	>10	0.393	0.535	>10	>10
2 Sunitinib	Approved 2 nd line	4.789	0.006	0.398	0.005	0.033
3 Regorafenib	Approved 3 rd line	9.953	0.231	0.290	0.033	0.114
4 Ripretinib	Ongoing clinical trials	8.037	0.031	0.013	0.037	0.098
5 Avapritinib	Ongoing clinical trials	4.075	0.292	0.017	0.860	4.952

All activity data are reported in μM and are the mean of at least n=2 determinations and have SEM within 0.2 log units.

1
2
3 We have previously reported on efforts to develop type II quinazoline based inhibitors of
4 both PDGFR and VEGFR that culminated in the discovery of AZD2932, **15**.²⁶ Follow up
5 work has also been described aimed at generating a PDGFR-selective agent from this
6 template which led to quinoline **16** (compound **23** in this referenced work).²⁷ We reasoned
7 that such inhibitors of PDGFR might show inhibition of some KIT mutants due to the close
8 homology of KIT and PDGFR, and the precedent established by compounds like **1**. What was
9 not clear however is whether the broad and selective profile we desired would be achievable
10 – the imatinib precedent also establishes that potent PDGFR inhibitors do not necessarily lead
11 to broad activity against KIT mutants. Testing of **15** in this panel (Table 2) highlighted that
12 AZD2932 did indeed show the desired broad spectrum of inhibition, but that it also carried
13 potent KDR activity, as it was designed to (encouragingly, no adverse signal was seen in the
14 parental line, suggesting little off target activity). Conversely, the PDGF-selective compound
15 **16**, despite weak effects on the KDR cell line, was a poor inhibitor of KIT mutants and also
16 showed some activity in the parental line. The challenge then was to understand if the potent
17 activity of analogues like **15** could be combined with good selectivity against KDR seen for
18 **16**, and work that led to the latter had highlighted the importance in the nature of the central
19 phenoxy ring and terminal heterocycle as being important drivers of KDR selectivity.
20 Compound **17** in which the phenoxy group is replaced with an anilino linker loses potency
21 against all KIT mutants, and also KDR (Table 3). The drop in potency against secondary A-
22 loop mutant D816H is almost identical to the drop in KDR potency (37- versus 39-fold) in
23 this instance. Adding a meta-methoxy group to the phenoxy ring in **18** results in maintenance
24 of KIT potency with a modest improvement in KDR selectivity, in line with SAR previously
25 reported for this series (selectivity of D816H over KDR is 17-fold, compared with almost
26 parity for **15**). Conversion of the central phenyl ring of **18** into a meta-pyridine **19** results in
27 significant diminishment of KDR potency, and greater selectivity over D816H at 45-fold,
28
29
30
31
32
33
34
35
36
37
38
39
40
41
42
43
44
45
46
47
48
49
50
51
52
53
54
55
56
57
58
59
60

1
2
3 although this does come with weaker overall D816H potency at 176 nM. Transposition of
4 this into its quinoline analogue **20** results in restoration of KIT mutant potency and
5 concomitant enhancement of selectivity over KDR (145-fold). The final compound in this
6 matrix, **21** combines the potent quinoline hinge binder with the meta-methoxy phenol linker
7 of **18**, to give single digit nanomolar inhibition of the three KIT lines, although in this
8 instance KDR selectivity has been substantially impacted. Testing of additional compounds
9 available from the original PDGFR program highlighted that other substituted end ring
10 heterocycles such as the 3-methylpyrazole found in **16** was not tolerated in c-KIT, and so
11 could not be used to drive further levels of KDR selectivity as had been done previously (data
12 not shown).
13
14
15
16
17
18
19
20
21
22
23
24
25
26
27

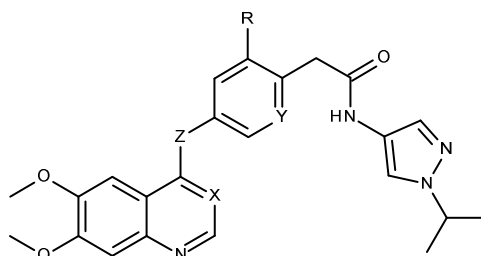
28 **Table 2.** Growth inhibition potency of literature AZ PDGFR inhibitors in KIT mutant Ba/F3 lines and effect on
29 KDR.



43
44
45
46
47
48
49
50

ID	Ba/F3 GI ₅₀ (μM)				KDR
	Parental	exon 11 del + V654A	exon 11 del + D816H	exon 11 del + T670I	
15 AZD2932	>10	0.012	0.070	0.004	0.093
16	4.289	0.685	0.786	1.918	2.674

51 All activity data are reported in μM and are the mean of at least n=2 determinations and have SEM within 0.2
52 log units.
53
54
55
56
57
58
59
60

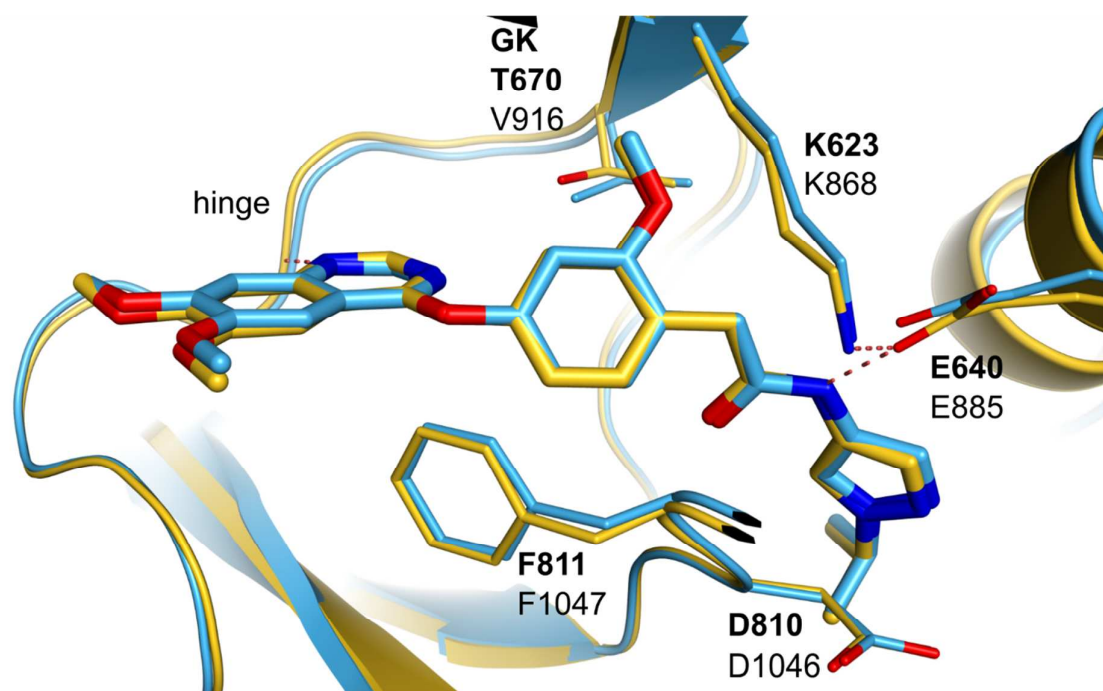
Table 3. SAR of KIT mutant Ba/F3 lines and effect on Tel-KDR selectivity

ID	X	Y	Z	R	Ba/F3 GI ₅₀ (μM)				KDR
					Parental	exon 11 del + V654A	exon 11 del + D816H	exon 11 del + T670I	
17	N	CH	NH	H	>10	0.337	2.592	0.078	3.595
18	N	CH	O	MeO	>10	0.008	0.026	0.012	0.442
19	N	N	O	MeO	>10	0.021	0.176	0.060	8.030
20	CH	N	O	MeO	>10	0.013	0.027	0.061	3.924
21	CH	CH	O	MeO	>10	0.006	0.008	0.007	0.077

All activity data are reported in μM and are the mean of at least n=2 determinations and have SEM within 0.2 log units.

In order to rationalise the observed selectivity margins for compounds **17-21**, we obtained X-ray crystal structures for compound **18**, bound to the kinase domain of both wild type KIT and KDR (see supplementary data for details). We did not attempt to crystallise in multiple KIT mutants, since we observed broad mutant selectivity over KDR and therefore reasoned that selective motifs, if apparent, would be revealed by contacts in the X-ray construct of KIT. There is high homology between KIT and KDR wild type sequences; the sequences are 56% identical in the kinase domains used for crystallography. A key difference between KIT and KDR lies in the gatekeeper residue, which is T670 in KIT and V916 in KDR. Other differences are more conservative, such as for hinge residues, which are Y672 (KIT) and

1
2
3 F918 (KDR). The binding modes of **18** in the overlaid kinase domains are shown in figure 2.
4
5 The binding poses are remarkably similar in the two kinases, with very few contacts to non-
6
7 conserved residues. The orientation of this ligand is as expected for a Type 2 kinase inhibitor.
8
9 The isopropyl group binds into the DFG pocket, with no distinction between KIT and KDR,
10
11 and the quinazoline nitrogen binds to the hinge. The two methoxy groups project out into
12
13 solvent. We speculate that the modest selectivity appears to arise from a less favourable
14
15 orientation of the central phenyl ring with respect to the gatekeeper V916 side chain of KDR,
16
17 relative to T670 in KIT. The orientation of the phenyl is dictated by the methoxy substituent
18
19 and hinders a binding mode which could optimise packing to V916 of KDR. The bound
20
21 ligand creates a poorly solvated cavity between ligand and gatekeeper, which can be
22
23 ameliorated in KIT by the more polar Thr side chain, with a favourable interaction between
24
25 quinazoline nitrogen and side chain hydroxyl.
26
27
28

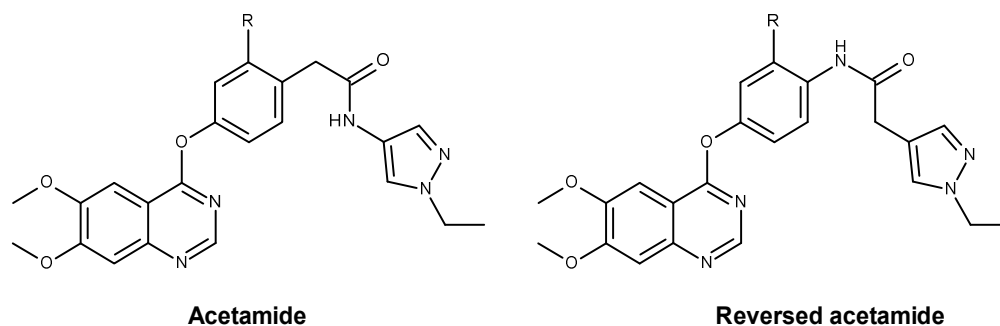


52 **Figure 2.** Kinase domains of KIT and KDR, overlaid on the binding site of Compound **18**. The KIT structure is
53 coloured yellow with labels in bold typeface, the KDR structure in blue with normal typeface. Side chains are
54
55
56
57
58
59
60

shown for the DFG motif and the catalytically important Glu-Lys pair, as well as the gatekeeper (GK) residue (PDB codes: 6GQJ and 6GQO).

We were motivated to explore the impact of reversing the acetamide linker in this series and so made reversed acetamide matched pairs to simple analogues available from the original PDGFR program (Table 4). Compound **22** is the *N*-ethylpyrazole analogue of **15**,^{16,26} and its reversed acetamide counterpart **23** encouragingly had a largely similar profile. Selectivity against KDR is moderately enhanced in the reversed acetamide, 6-fold from roughly 1:1 over D816H, while affinity for the T670I gatekeeper is most severely impacted (down 20-fold), activity against V654A and D816H are largely similar. Analogue **24**, in which the central ring is appended with a methoxy group, is a first indication however that the SAR that was apparent in the original acetamide series does not transfer when the acetamide is reversed. Whereas previously a 17-fold improvement in selectivity was noted, here selectivity is unchanged, as is potency across all the mutants – methoxy on the central ring appears to offer no advantage. A similar breakdown in SAR was seen for introduction of a central pyridine ring (Table 5). In the quinoline matched pairs **25** (phenyl) and **26** (pyridine), introduction of nitrogen causes a significant drop in all KIT potencies except T670I, and although KDR potency is weaker, selectivity is unchanged.

Table 4. Impact of reversing the acetamide linker on KIT and KDR potency.



ID	Amide	R	Ba/F3 GI ₅₀ (μM)				KDR
			Parental	exon 11 del + V654A	exon 11 del + D816H	exon 11 del + T670I	
22	Acetamide	H	>10	0.044	0.488	0.007	0.680
23	Reversed acetamide	H	>10	0.021	0.250	0.141	1.615
24	Reversed acetamide	MeO	>10	0.078	0.251	0.086	2.551

All activity data are reported in μM and are the mean of at least n=2 determinations and have SEM within 0.2 log units.

We obtained a matched pair of X-ray structures for compound **23**, as shown in figure 3. In this case, we observed ligand binding modes which are slightly offset in the vicinity of the hinge and gatekeeper, with the pendant ethyl group of the pyrazole ring coincident in the two binding sites. This suggests that interaction in the DFG pocket is dominant for this scaffold, but that selectivity arises once again from the gatekeeper pocket. Since **23** is a quinazoline, the N3 atom is available to chelate a water molecule, which is now visible in the KIT structure (shown as a red sphere). There is no water observed in KDR here, our assumption being that this would be very unstable when packed against the V918 side chain. Instead, in KDR, the ligand partially occupies the solvent pocket in preference to water, weakening both the hinge interaction and the packing against the gatekeeper residue. We assumed that a similar solvation stabilisation of **18** is possible, but this was not observed in our X-ray structures (figure 2). The nitrogen position in the reversed acetamide precludes a direct hydrogen bond with the glutamic acid chain (E640/E885), in contrast to that observed in the normal acetamide. This region of the complex remains quite polar however, so that a crystallographic water is observed to bind in both CKIT and KDR, as shown in Figure 3. The water appears to mediate an interaction between acid side chain and ligand. The water

positions are almost coincident in CKIT and KDR, so that we could not use this interaction to explain selectivity between the two proteins.

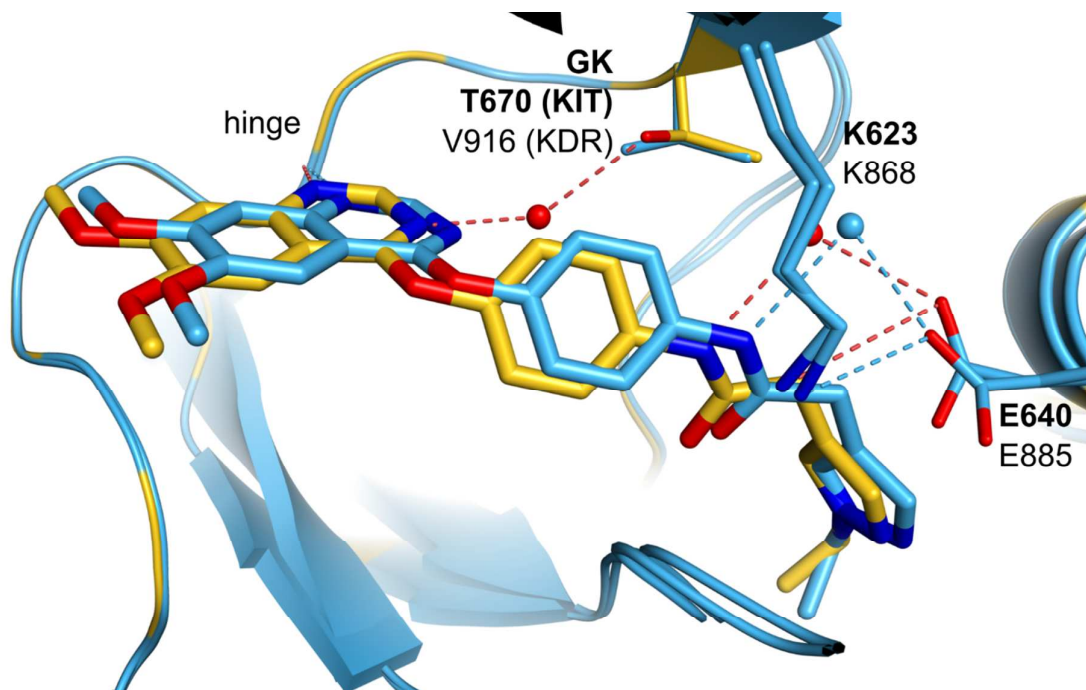
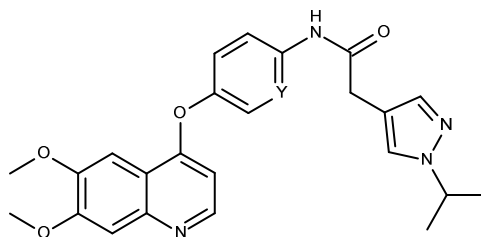


Figure 3. Kinase domains of KIT and KDR, overlaid on the binding site of reversed acetamide compound **23**. KIT protein ribbons are coloured by sequence identity, with blue residues identical and yellow non-identical to KDR. The binding mode is offset between the two kinases, but there are still very few contacts to non-conserved residues. Water molecules are shown as red spheres in KIT and blue spheres in KDR). A water molecule is observed in the KIT structure, but is absent from the KDR structure. Selectivity appears to arise from less favourable orientation of the central aromatic ring against the V916 side chain of KDR, relative to the solvated T670 side of KIT. In addition, the hinge interaction in KDR seems to be less optimal than for KIT. (PDB codes: 6GQK and 6GQP)

Table 5. Impact of reversing a pyridine linker on KIT and KDR potency.



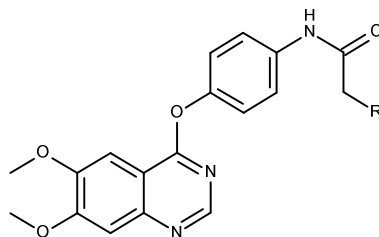
ID	Y	Ba/F3 GI ₅₀ (μM)				KDR
		Parental	exon 11 del + V654A	exon 11 del + D816H	exon 11 del + T670I	
25	CH	>10	0.026	0.047	0.007	0.082
26	N	>10	0.150	0.518	0.008	0.761

All activity data are reported in μM and are the mean of at least n=2 determinations and have SEM within 0.2 log units.

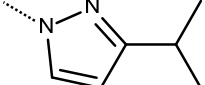
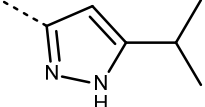
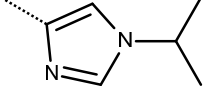
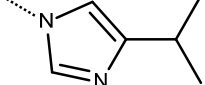
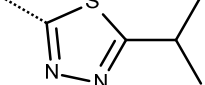
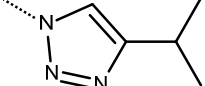
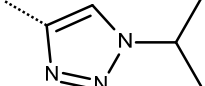
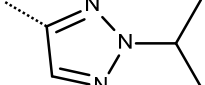
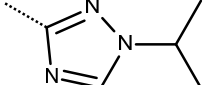
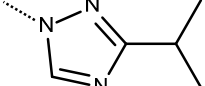
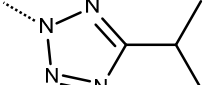
With previous SAR unsuited to driving the greater levels of potency and selectivity required, we turned attention to varying the end-ring of the reversed acetamide using a series of aromatic acetic acids available through an in house building block initiative.²⁸ Table 6 shows the impact of varying the nature of the 5-membered heteroaromatic portion of the molecule, and here we focused on finding the optimal balance of exon 11 deletion + D816H potency (since this appears the most challenging mutant to inhibit with this template) and KDR selectivity, whilst keeping LogD as low as possible. Compound **27**, serves as a useful benchmark for these changes as it is the reversed acetamide version of analogue **15** – potency and lipophilicity are good, but KDR selectivity is modest. Switching the isopropyl group to a difluoromethyl **28** gives a largely similar profile. Reversing the pyrazole so that connection to the acetamide is via an *N*-link as in analogues **29** and **30** provides compounds with improved KDR margin but comes at the expense of increased lipophilicity. The last pyrazole in this set **31** with a free *NH* gives a very potent D816H inhibitor, reasonable selectivity but again with higher than desirable LogD of 3.6. A C-linked imidazole **32** sees a drop in activity and

selectivity, whereas linking through nitrogen as in **33** gives a potent and selective inhibitor. A thiadiazole **34** is potent but has only 10-fold margin to KDR and LogD of 3.3. We also examined a series of 1,2,3-triazoles **35** – **37**. The pick of these appears to be triazole **35**, which combines good potency (19 nM) and selectivity with an acceptable LogD of 2.9. Triazole **36** is less potent and triazole **37** less selective than **35**. In related 1,2,4-triazoles, compound **38** sees potency significantly diminished, and analogue **39**, although an improvement, is not superior to any 1,2,3-triazole. Completing this set, the tetrazole **40** shows a reasonable balance of potency, selectivity and lipophilicity. From this work *N*-linked triazole **35** emerged as the most favourable end-ring, although further increases in selectivity were desired.

Table 6. Exon 11 deletion + D816H KIT mutant potency and KDR selectivity for a series of aromatic acetamides.



ID	R	exon 11 del D816H Ba/F3 GI ₅₀ (μM) ¹	Fold KDR selectivity	LogD ²
27		0.021	5.9	2.9
28		0.087	4.4	2.7
29		0.021	11.4	3.8

1					
2					
3					
4	30		0.035	23.5	3.5
5					
6					
7					
8	31		0.009	15.6	3.6
9					
10					
11					
12	32		0.240	4.6	2.8
13					
14					
15					
16	33		0.021	34.1	3.3
17					
18					
19					
20	34		0.026	9.9	3.3
21					
22					
23					
24	35		0.019	32.2	2.9
25					
26					
27					
28	36		0.111	12.6	2.6
29					
30					
31					
32	37		0.075	9.3	2.9
33					
34					
35					
36	38		1.369	3.9	2.3
37					
38					
39					
40	39		0.175	15.9	2.6
41					
42					
43					
44	40		0.042	15.7	3.0
45					
46					

¹ All activity data are reported in μM and are the mean of at least $n=2$ determinations and have SEM within 0.2

log units. ² Measured LogD at $\text{pH}_{7.4}$.

1
2
3 The notable gains in potency and selectivity for these heterocyclic end groups prompted us to
4 solve a further X-ray matched pair, this time for compound **35**. As seen in figure 4, the
5 binding mode at the hinge and gatekeeper is less offset than for **23** (figure 3), but this appears
6 to be due to a different orientation in the DFG pocket. The pendant isopropyl group packs
7 against the V898 side chain of KDR but projects further from the pocket in KIT due to a
8 larger I653 side chain at the equivalent position. This results in a significant offset of the
9 triazolo group between KIT and KDR and a different orientation for the isopropyl group. The
10 triazole dipole is oriented towards bulk water, as we would expect for a broadly hydrophobic
11 pocket and consequently solvent mapping suggests that the triazolo motif occupies a more
12 favourable position in KIT relative to KDR.²⁹ In KDR, it appears to be buried too far into the
13 pocket, to optimise packing against V898, precluding effective solvation of the exposed
14 dipole. This also explains why compound **27** is less selective, since the pyrazole end group
15 can present a hydrophobic atom in the KDR pocket. Combining isopropyl with a heterocycle
16 with significant dipole, such as triazolo, gives a binding orientation which is optimal for
17 solvation in the KIT pocket and sub-optimal for KDR. When coupled with a selective
18 gatekeeper motif and the bound water (also visible in figure 2), we then see a significant
19 selectivity gain.
20
21
22
23
24
25
26
27
28
29
30
31
32
33
34
35
36
37
38
39
40
41
42
43
44
45
46
47
48
49
50
51
52
53
54
55
56
57
58
59
60

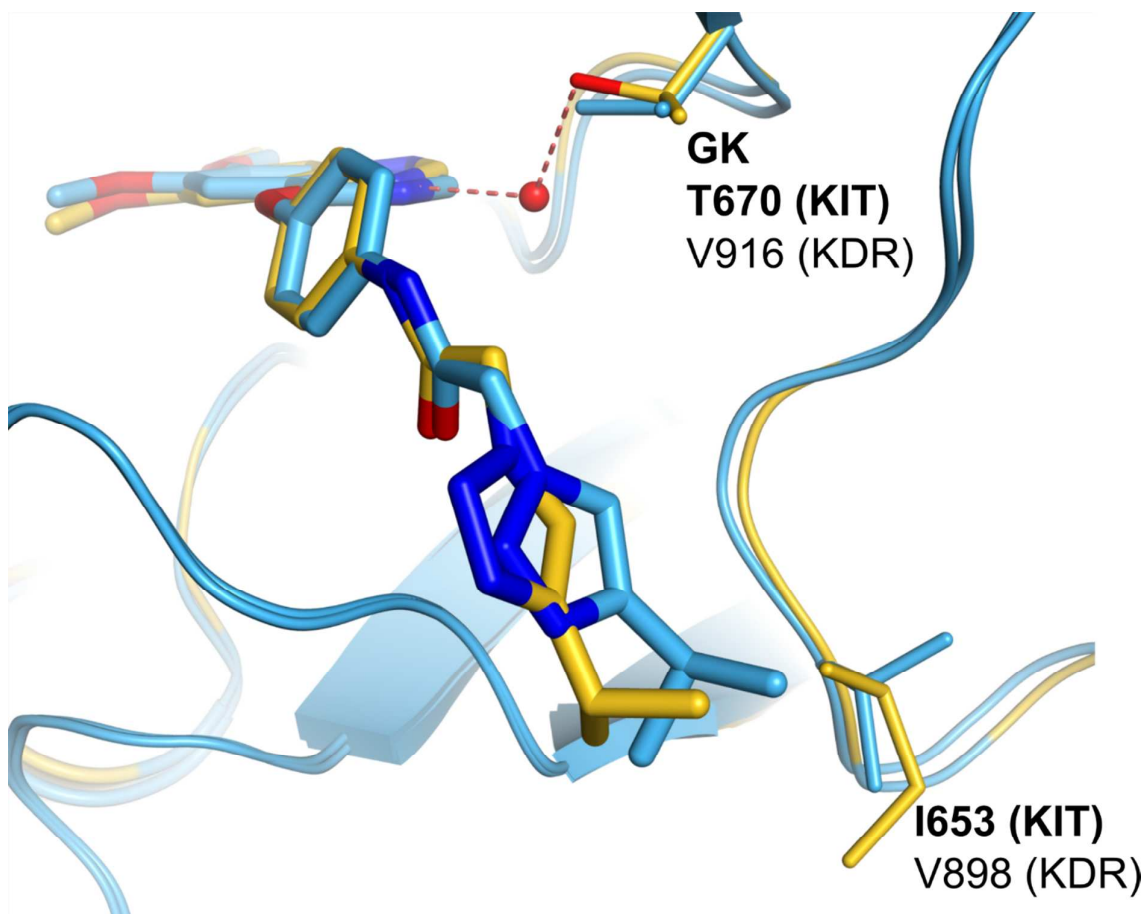


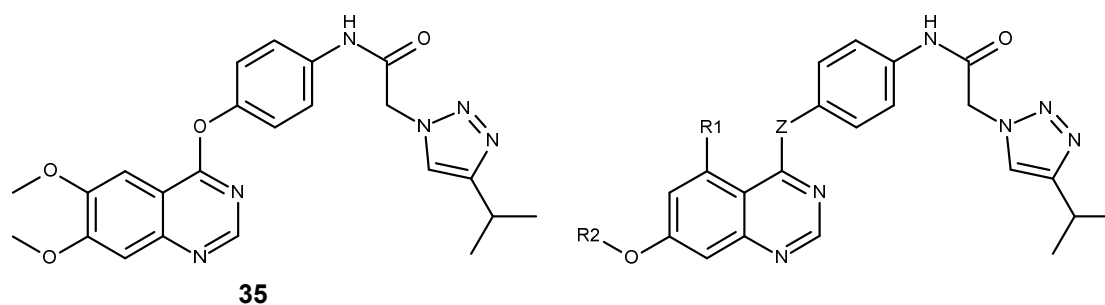
Figure 4. Kinase domains of KIT and KDR, overlaid on the binding site of compound **35**. KIT protein is coloured by sequence identity, with blue residues identical and yellow non-identical to KDR. The binding mode at hinge and gatekeeper is less offset than in previous examples, but attention now shifts to non-conserved residues in the DFG pocket. The isopropyl group clashes with I653 in KIT, but is accommodated by the smaller V898 side chain of KDR. The triazolo motif is more buried in KDR as a result and we hypothesise that this results in a desolvation penalty which increases affinity to KIT for this ligand and for this general DFG pocket motif. (PDB codes: 6GQL and 6GQQ).

We next turned our attention to examining substituents at the quinazoline 5-position, since this is a region that projects towards the ribose pocket of ATP, an area of fruitful optimisation in quinazoline-based kinase inhibitors historically.³⁰ Compound **35** is a potent inhibitor of all three KIT mutants (Table 7). Migration of the 6-methoxy group to the 5-position **41** does not

1
2
3 change the profile a great deal – a modest 2 to 3-fold drop in potencies are observed across all
4
5 cell lines, and certainly KDR selectivity is not further enhanced. Despite this, we explored the
6
7 impact of switching the 4-phenoxy linker back to a 4-anilino linker with compound **42**. We
8
9 had seen earlier in the normal amide series, compound **17** with an anilino linker lost
10
11 significant activity against KIT mutants, although we speculated that the potential lone pair
12
13 clash between the adjacent oxygen atoms (at C4 and C5) in **41** might impact the optimal C4
14
15 substituent vector, and that reversion to an *NH* linker, which could internally hydrogen bond
16
17 to the 5-methoxy group, might be more favourable. In the event, the aniline linked **42** was as
18
19 effective at inhibiting KIT mutants as its phenoxy counterpart, but with much improved
20
21 selectivity over KDR (113-fold compared with 24- and 32-fold for **41** and **35** respectively). It
22
23 is striking that two structural changes that individually lead to a worsened profile, when
24
25 combined together are able to drive a significant benefit. Exploration of alternative
26
27 substituents at C5 led to 5-fluoro analogue **43** which maintains KIT potency and leads to even
28
29 greater KDR selectivity of at least 400-fold. Fluorine was selected as an alternative to
30
31 methoxy that could, potentially at least, form an internal hydrogen bond to the C4 *NH*. This
32
33 compound however unexpectedly suffered from adverse physicochemical properties, in
34
35 particular high plasma protein binding of 99.7% bound, an issue that was directly addressed
36
37 by variation of the C7 substituent. Compound **44**, containing a C7 methoxyethoxy group was
38
39 determined to have the optimal balance between KIT mutant potency and KDR selectivity
40
41 from this work and was selected for further profiling. It demonstrates very potent growth
42
43 inhibition across KIT mutant cell lines with good KDR margin – not quite as selective as **43**,
44
45 but significant improvements in physicochemical and ADME properties (Table 8). Despite a
46
47 low solubility consistent with its chemical structure and neutral chemotype, permeability in
48
49 Caco2 cells is very high. This, coupled with its low in vitro clearance in hepatocytes leads to
50
51 excellent observed in vivo pharmacokinetics in preclinical species. Bioavailability is high,
52
53
54
55
56
57
58
59
60

and clearance low across all of mouse, rat and dog. Volume of distribution is low consistent with the neutral structure. A structure of **44** bound in KIT was obtained and shows features consistent with the preceding X-ray structures (figure 5). There is a bound water at the gatekeeper, promoting selectivity, and the triazolo group binds in a similar place in the DFG pocket as was seen for compound **35**. The extended C7 side chain protrudes from the active site out into solvent.

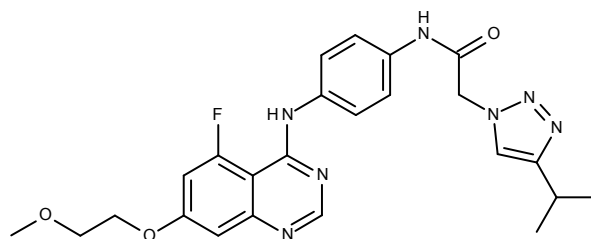
Table 7. SAR of 5-substituted quinazolines.



ID	Z	R1	R2	Ba/F3 GI ₅₀ (μM)				KDR
				Parental	exon 11 + del V654A	exon 11 + del D816H	exon 11 + del T670I	
35				>10	0.003	0.019	0.017	0.612
41	O	MeO	Me	>10	0.007	0.050	0.055	1.222
42	NH	MeO	Me	>10	0.003	0.048	0.107	5.408
43	NH	F	Me	>10	0.002	0.025	0.068	>10
44	NH	F	MeO(CH ₂) ₂	>10	0.003	0.009	0.016	1.378

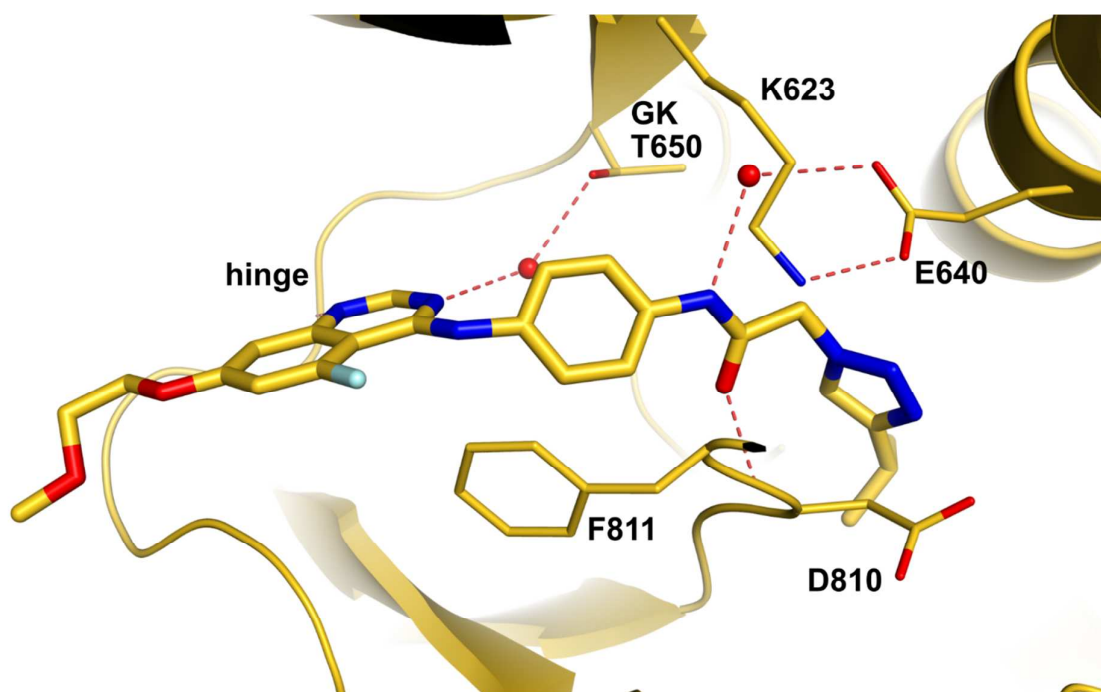
All activity data are reported in μM and are the mean of at least n=2 determinations and have SEM within 0.2 log units.

Table 8. Detailed ADME characteristics of compound **44**.



Parameter	Value	
LogD $pH7.4$ ¹	3.0	
Solubility $pH6.5$ (μM) ²	6	
Permeability Caco2 A to B ($1E^{-6}$ cm/s) ³ (efflux ratio)	62.3 (2.6)	
Plasma protein binding % free (mouse, rat, dog, human)	4.9, 2.2, 6.8, 3.5	
Hepatocyte Clint ($\mu l/min/10^{-6}$ cells) (mouse, rat, dog, human)	5, 17, <1, <1	
hERG IC ₅₀ (μM)	>33.3	
Pharmacokinetics Cl(ml/min/kg), Vd _{ss} (l/kg), t _{1/2} (h), F%	Mouse ⁴	7, 0.7, 2, 100
	Rat ⁵	8, 0.6, 3, 79
	Dog ⁶	2, 0.3, 4, 69

¹Measured LogD at $pH7.4$. ²Solubility of crystalline Form A measured in $pH6.5$ phosphate buffer at $37^{\circ}C$
³Permeability measured at $pH6.5$ using 10 μM solution of compound. ⁴PK in CD1 Mouse following oral (21 $\mu Mol/kg$) and iv doses (10 $\mu Mol/kg$). ⁵PK in Han Wistar Rat following oral (2.1 $\mu Mol/kg$) and iv doses (1 $\mu Mol/kg$). ⁶PK in Dog following oral (2.1 $\mu Mol/kg$) and iv doses (1 $\mu Mol/kg$). Half lives reported are from oral dosing.



1
2
3 **Figure 5.** Co-crystal structure of **44** bound to c-KIT. (resolution 2Å). Water molecules shown as red spheres.
4 PDB code: 6GQM.
5
6
7
8
9

10 Compound **44** was compared against the approved and investigational KIT inhibitors outlined
11 in Figure 1 against a much broader panel of KIT mutant Ba/F3 cell lines expressing a diverse
12 set of clinically relevant primary and secondary mutations, including a small panel of PDGFR
13 driven lines relevant in subsets of GIST (Table 9). It shows very potent growth inhibition of
14 nearly all mutants tested and consistent with its lineage and other KIT inhibitors, maintains
15 potent activity against PDGFR, including the clinically GIST-relevant D842V mutant. It
16 maintains low nM potency against secondary mutations on a primary background of either
17 exon 9 insertion or exon 11 deletion and is sub-10 nM in 12 of the 19 lines examined.
18 Conversely, imatinib **1** is a relatively poor inhibitor of these diverse KIT mutants, showing
19 significant activity against a primary mutation of exon 11 insertion and V560D, together with
20 PDGFR only. Sunitinib **2** carries greater KIT mutant activity than **1** and shows potent activity
21 against secondary mutations of ATP binding pocket, but is much weaker against clinically
22 relevant mutations of the A-loop. Third line agent regorafenib **3** is a little more potent against
23 these mutations but against many of the others appears inferior to sunitinib **2**. The
24 investigational agent ripretinib **4** does show potent and broad-spectrum activity against the
25 KIT mutants in this panel, although with the exception of its PDGF activity it is only superior
26 to **44** in a single mutant (primary D816V). As previously indicated, the margin to KDR for
27 this agent is significantly eroded relative to **44** (only 8-fold compared with 153-fold against
28 exon 11 insertion + D816H). Avapritinib **5** is potent against certain subsets of KIT mutants,
29 notably D816/820 and PDGFR, although lacks potent activity against mutants such as V654A
30 and T670I. Consistent with our goals, compound **44** demonstrates equivalent or superior
31 growth inhibition in all but 2 of the 19 cell lines investigated when compared to agents **1** to **5**.
32
33
34
35
36
37
38
39
40
41
42
43
44
45
46
47
48
49
50
51
52
53
54
55
56
57
58
59
60

Table 9. Comparison of mutant KIT and PDGF potencies for compound **44** with approved and investigational GIST therapies **1 - 5**.

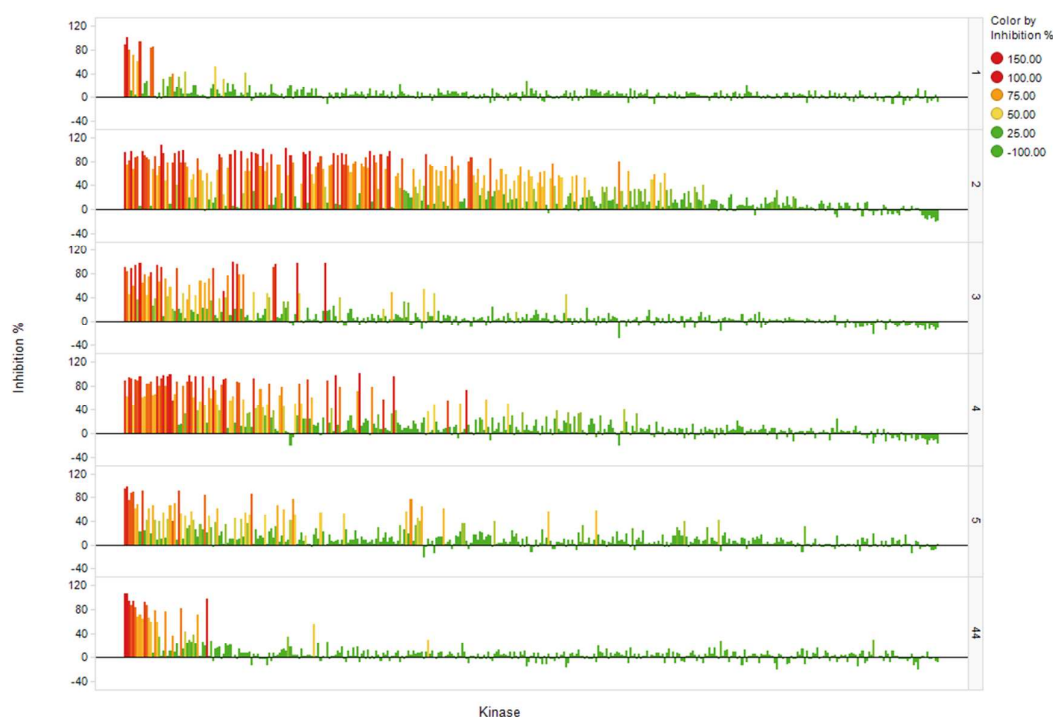
Gene	Primary mutation	Secondary Mutation	KIT inhibitor Ba/F3 GI ₅₀ (μM)					
			44	1	2	3	4	5
KIT	Exon 9 ins ¹	-	0.002	0.192	0.007	0.114	0.034	0.167
	Exon 9 ins ¹	V654A	0.022	3.947	0.012	1.270	0.205	0.751
	Exon 9 ins ¹	D816H	0.051	2.749	0.584	0.833	0.078	0.069
	Exon 11 del ²	-	0.001	0.017	0.004	0.021	0.004	0.078
	Exon 11 del ²	V654A	0.003	0.392	0.006	0.234	0.032	0.292
	Exon 11 del ³	V654A	0.008	1.523	0.024	0.943	0.130	0.117
	Exon 11 del ²	T670I	0.016	9.689	0.005	0.034	0.038	0.860
	Exon 11 del ²	D816H	0.009	0.537	0.400	0.297	0.013	0.017
	Exon 11 del ²	D820A	0.003	0.216	0.214	0.063	0.006	0.019
	Exon 11 del ²	Y823D	0.014	0.669	0.782	0.094	0.014	
	Exon 11 del ²	N822K	0.003	0.223	0.271	0.049	0.004	0.034
	Exon 11 del ²	A829P	0.004	0.312	0.430	0.047	0.003	0.028
	V560D	-	0.001	0.070	0.027	0.108	0.023	0.042
	V560D	V654A	0.007	0.701	0.007	0.549	0.075	0.427
	V560D	D816H	0.018	1.191	0.696	0.834	0.048	0.029
D816V	-	0.971	9.930	0.638	2.371	0.037	0.008	
PDGFR	Tel-PDGFR α		0.001	0.046	0.030	0.051	0.040	0.034
	Tel-PDGFR β		0.008	0.102	0.114	0.029	0.045	0.022
	V561D ⁴	D842V ⁴	0.022	0.567	0.631	0.522	0.188	0.010

¹ AY502-503 insertion at exon 9. ² Deletion of 557-558 at exon 11. ³ Deletion of 560-578 at exon 11. ⁴

PDGFR α

In order to ensure that the broad KIT mutant inhibition profile observed had not been achieved at the expense of general kinome selectivity, compound **44** was assessed in an

1
2
3 extended panel of human kinase binding assays alongside clinical agents **1** – **5** (Figure 6). In
4
5 this panel of 379 human kinases, activity was compared by screening at a single, relatively
6
7 high concentration of 1 μM , which is far in excess of the potency seen in the Ba/F3 GI_{50}
8
9 assays. Encouragingly compound **44** compares well to these other inhibitors, with an overall
10
11 selectivity similar to that of imatinib **1** and avapritinib **5**. Both Sunitinib **2** and regorafenib **3**
12
13 show increased activity across this panel, with exploratory agent ripretinib **4** showing a
14
15 spectrum of activity between these two approved therapies.
16
17
18
19
20
21



22
23
24
25
26
27
28
29
30
31
32
33
34
35
36
37
38
39
40
41
42
43
44
45 **Figure 6.** Comparative selectivity of inhibitors **1** – **5** and **44** in a panel of 379 human kinases run in the
46
47 SelectScreen kinase panel at ThermoFisher Scientific at a single concentration of 1 μM . This data is available as
48
49 individual annotated kinase datapoints in Supporting Information.
50
51
52
53
54
55
56
57
58
59
60

1
2
3 A key advantage of using Ba/F3 cell lines in the cascade optimisation is that these allow a
4 direct assessment of potency translation *in vivo*. The activity of compound **44** in a series of
5 mouse allograft tumor models using these Ba/F3 lines was assessed and compared to current
6 standards of care relevant to each mutant (Figure 7 and Table 10). As expected **1** shows only
7 limited activity in the exon 11 del/D816H background a mutation to which it is refractory.
8 Regorafenib **3** fares better and is able to drive regression of tumour volume at a dose of 100
9 mg/kg qd, although this is surpassed by **44** at a dose of 20 mg/kg bid. A dose response is
10 evident in that **44** at a dose of 2 mg/kg bid shows no impact on tumour size. Sunitinib **2** was
11 not assessed in this model as it is inactive against the D816H mutant. In an exon 11
12 del/V654A allograft however and consistent with its clinical use, **2** showed strong regressions
13 at 80 mg/kg qd, and was matched by **44** at a dose of 20 mg/kg bid (and even as low as 2
14 mg/kg **44** was highly effective). Imatinib showed moderate activity in this study. Figure 8
15 shows the pharmacodynamic response to **44** in the D816H model at the top 20 mg/kg dose
16 tested with the impact on levels of pKIT and downstream markers pERK and pAKT, together
17 with a timecourse of compound free cover levels above IC₉₀ in the same study. Following a
18 single dose, high free cover over target is achieved and is associated with complete
19 suppression of pKIT and downstream markers out to 8 hours. As compound is cleared and
20 cover declines, these signals recover although recovery is not complete even at 24 hours.
21
22
23
24
25
26
27
28
29
30
31
32
33
34
35
36
37
38
39
40
41
42
43
44
45
46
47
48
49
50
51
52
53
54
55
56
57
58
59
60

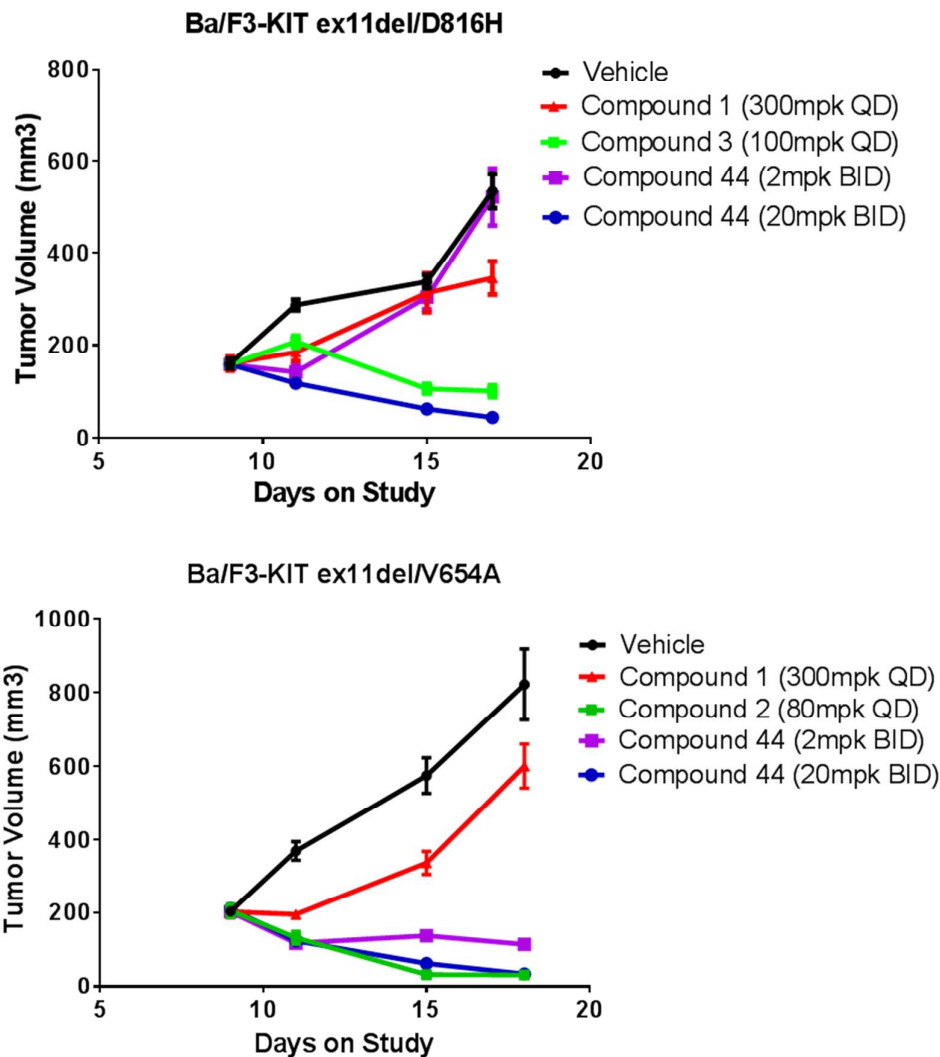


Figure 7. The in vivo efficacy of KIT inhibitors in mouse allograft disease models. Upper panel: Imatinib and regorafenib versus **44** in an exon 11 del/D816H model. Lower panel: Imatinib and sunitinib versus **44** in an exon 11 del/V654A model. Doses for standards of care were selected to best represent their clinically relevant doses.

Table 10. Percent and statistical significance of tumor growth inhibition and regressions of **44** relative to vehicle and standards of care in two mouse allograft disease models of mutant KIT activity.

Tumor	ID	Dose (mg/kg)	Schedule	Route	% Inhibition ¹	% Regression ¹	p-value ²
Ba/F3 KIT-exon 11 del/D816H	vehicle	n/a	BD	p.o	n/a	n/a	n/a
	1	300	QD	p.o	43	0	0.0095

	3	100	QD	p.o	>100	39	<0.0001
	44	2	BD	p.o	5	0	0.3818
	44	20	BD	p.o	>100	75	<0.0001
	vehicle	n/a	BD	p.o	n/a	n/a	n/a
	1	300	QD	p.o	34	0	0.0495
Ba/F3 KIT-exon 11 del/V654A	2	80	QD	p.o	>100	87	<0.0001
	44	2	BD	p.o	>100	44	<0.0001
	44	20	BD	p.o	>100	85	<0.0001

¹ On last day of dosing. ² Relative to vehicle.

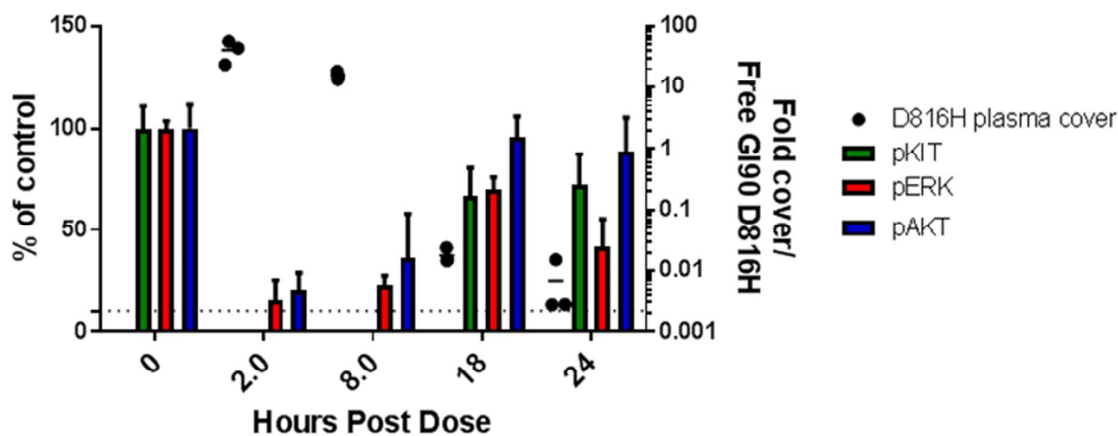


Figure 8. Pharmacodynamic effect of 44 on tumor pKIT, pERK and pAKT in an exon 11 del/D816H mouse allograft model from a single dose of 20 mg/kg po. No pKIT was detectable at $t=2$ or 8 hours. A more detailed statistical analysis of this data is available in Supporting Information.

Conclusions

Having established as a goal the challenging profile of an inhibitor capable of addressing all diverse KIT mutants, this has been realised in a series of type II quinazoline kinase inhibitors. Identification of a series of kinase inhibitors from an historical project, combined with structure-based insights allowed for rapid optimisation in particular of both mutant and kinase

1
2
3 selectivity, not just against KDR but the wider kinome. Despite high homology between KIT
4 and anti-target KDR, we propose that subtle differences in the way each is able to
5 accommodate and in particular solvate the liganded structures is key to the enhanced
6 selectivity seen. The pre-clinical in vivo efficacy of **44**, now designated AZD3229 is
7 encouraging, particularly in relation to current standards of care and may hold promise in the
8 future treatment of GIST patients. Further data relating to the pharmacological activity of
9 AZD3229, including assessment of required margins over KDR to ensure no hypertensive
10 effects³¹ that limit current agents will be reported in due course.
11
12
13
14
15
16
17
18
19
20
21
22

23 **Experimental Methods**

24
25
26 **Chemistry** Unless otherwise stated, commercially available reagents were used as supplied.
27 All reactions requiring anhydrous conditions were conducted in dried apparatus under an
28 atmosphere of nitrogen. Flash column chromatography was performed on Merck Kieselgel
29 silica (Art. 9385) or on reversed phase silica (Fluka silica gel 90 C18) or on Silicycle
30 cartridges (40-63 μm silica, 4 to 330 g weight) or on Grace resolv cartridges (4 – 120 g) or on
31 RediSep Rf 1.5 Flash columns or on RediSep Rf high performance Gold Flash columns (150
32 – 415 g weight) or on RediSep Rf Gold C18 Reversed-phase columns (20 – 40 μm silica)
33 either manually or automated using an Isco CombiFlash Companion system or similar
34 system. Preparative reverse phase HPLC was performed on a Waters instrument (600/2700 or
35 2525) fitted with a ZMD or ZQ ESCi mass spectrometers and a Waters X-Terra or a Waters
36 X-Bridge or a Waters SunFire reverse-phase column (C-18, 5 microns silica, 19 mm or 50
37 mm diameter, 100 mm length, flow rate of 40 ml / minute) using decreasingly polar mixtures
38 of water (containing 1% ammonia) and acetonitrile or decreasingly polar mixtures of water
39 (containing 0.1% formic acid) and acetonitrile as eluents. NMR chemical shift values were
40
41
42
43
44
45
46
47
48
49
50
51
52
53
54
55
56
57
58
59
60

1
2
3 measured on the delta scale [proton magnetic resonance spectra were determined using a
4 Bruker Avance 500 (500 MHz), Bruker Avance 400 (400 MHz), Bruker Avance 300 (300
5 MHz) or Bruker DRX (300 MHz) instrument]; measurements were taken at ambient
6 temperature unless otherwise specified; the following abbreviations have been used: s,
7 singlet; d, doublet; t, triplet; q, quartet; m, multiplet; dd, doublet of doublets; ddd, doublet of
8 doublet of doublet; dt, doublet of triplets; bs, broad signal. In general, end products were also
9 characterized by mass spectroscopy following liquid chromatography (LCMS or UPLC); in
10 general, reverse-phase C18 silica was used with a flow rate of 1 ml / minute and detection
11 was by Electrospray Mass Spectrometry and by UV absorbance recording a wavelength range
12 of 220-320 nm. Analytical UPLC was performed on CSH C18 reverse-phase silica, using a
13 Waters XSelect CSH C18 column with dimensions 2.1 x 50mm and particle size 1.7 micron).
14 Gradient analysis was employed using decreasingly polar mixtures as eluent, for example
15 decreasingly polar mixtures of water (containing 0.1% formic acid or 0.1% ammonia) as
16 solvent A and acetonitrile as solvent B. A typical 2 minute analytical UPLC method would
17 employ a solvent gradient over 1.3 minutes, at approximately 1 ml per minute, from a 97:3
18 mixture of solvents A and B respectively to a 3:97 mixture of solvents A and B. The
19 reported molecular ion corresponds to the [M+H]⁺ unless otherwise specified; for molecules
20 with multiple isotopic patterns (Br, Cl, etc.) the reported value is the one obtained for the
21 lowest isotope mass unless otherwise specified. Ion exchange purification was generally
22 performed using an SCX-2 (Biotage) cartridge. Where reactions refer to the use of a
23 microwave, one of the following microwave reactors were used: Biotage Initiator, Personal
24 Chemistry Emrys Optimizer, Personal Chemistry Smithcreator or CEM Explorer. Purities
25 were assessed using LCMS by UV absorbance and ¹H NMR and are ≥ 95% unless otherwise
26 stated.
27
28
29
30
31
32
33
34
35
36
37
38
39
40
41
42
43
44
45
46
47
48
49
50
51
52
53
54
55
56
57
58
59
60

1
2
3 **Ethyl 2-(4-isopropyl-1*H*-1,2,3-triazol-1-yl)acetate (7).** A 30% solution of ethyl 2-
4 azidoacetate (6) in DCM (19.5 g, 45.4 mmol) was added as a solution in acetonitrile (27 ml)
5 over 5 minutes to a suspension of copper(I) iodide (0.17 g, 0.9 mmol), 3-methylbut-1-yne
6 (5.1 ml, 49.9 mmol) and triethylamine (0.13 ml, 0.9 mmol) in acetonitrile (27 ml) at room
7 temperature. The mixture was stirred for 3 days at room temperature. The mixture was
8 concentrated and the residue was partitioned between water (150 ml) and ethyl acetate (150
9 ml). The aqueous layer was extracted with ethyl acetate (100 ml) and the extracts combined
10 with the organic layer. The combined extracts were dried and evaporated to dryness. The
11 crude product was purified by flash silica chromatography, elution gradient 30 to 50% ethyl
12 acetate in heptane. Pure fractions were evaporated to dryness to afford the title compound as
13 a white crystalline solid (8.06 g, 90%). ¹H NMR (500 MHz, DMSO, 27°C) δ 1.21 (3H, t),
14 1.22 (6H, d), 2.98 (1H, hept), 4.16 (2H, q), 5.30 (2H, s), 7.82 (1H, d); m/z: ES+ [M+H]⁺ 198.

15
16
17
18
19
20
21
22
23
24
25
26
27
28 **2-(4-Isopropyl-1*H*-1,2,3-triazol-1-yl)acetic acid (8).** Lithium hydroxide hydrate (10.2 g,
29 242.5 mmol) was added as a solution in water (540 ml) to ethyl 2-(4-isopropyl-1*H*-1,2,3-
30 triazol-1-yl)acetate (7) (15.9 g, 80.8 mmol) in THF (180 ml). The mixture was stirred for 90
31 minutes, then concentrated. The resulting aqueous solution was acidified to pH 5 with 2M
32 HCl and extracted with ethyl acetate (200 ml). The aqueous layer was evaporated to dryness
33 to afford the title compound as a white solid containing LiCl (28.2 g, 100%, 48% strength),
34 which was used without further purification. ¹H NMR (500 MHz, DMSO, 27°C) δ 1.20 (6H,
35 d), 2.92 (1H, hept), 4.59 (2H, s), 7.62 (1H, d); m/z: ES+ [M+H]⁺ 170.

36
37
38
39
40
41
42
43
44
45
46 ***Tert*-Butyl (4-(2-(4-isopropyl-1*H*-1,2,3-triazol-1-yl)acetamido)phenyl)carbamate (9).**
47 HATU (18.4 g, 48.3 mmol) was added to a solution of *tert*-butyl (4-aminophenyl)carbamate
48 (8.4 g, 40.3 mmol), 2-(4-isopropyl-1*H*-1,2,3-triazol-1-yl)acetic acid (8) (19.4 g, 44.3 mmol)
49 and DIPEA (10.5 ml, 60.4 mmol) at ambient temperature. The mixture was stirred at ambient
50 temperature for 16 hours. The mixture was concentrated to 75 ml volume, diluted with water
51
52
53
54
55
56
57
58
59
60

(700 ml) and extracted with ethyl acetate (3x 300 ml). The combined ethyl acetate extracts were washed with 0.5M citric acid solution (300 ml), water (4x 300 ml), 0.5M NaHCO₃ solution (200 ml), water (200 ml), brine (200 ml) and dried. The solution was evaporated to dryness and the residue was recrystallised from acetonitrile to afford the title compound as a white solid (8.2 g, 57%). ¹H NMR (500 MHz, DMSO, 27°C) δ 1.23 (6H, d), 1.45 (9H, s), 2.98 (1H, hept), 5.20 (2H, s), 7.38 (2H, d), 7.44 (2H, d), 7.83 (1H, d), 9.27 (1H, s), 10.31 (1H, s). *m/z*: ES+ [M+H]⁺ 360.

***N*-(4-Aminophenyl)-2-(4-isopropyl-1*H*-1,2,3-triazol-1-yl)acetamide (10).** 4M Hydrogen chloride in dioxane (15.3 ml, 61.2 mmol) was added to a mixture of *tert*-butyl (4-(2-(4-isopropyl-1*H*-1,2,3-triazol-1-yl)acetamido)phenyl)carbamate (**9**) (2.2 g, 6.1 mmol) in DCM (20 ml) and methanol (20 ml). The mixture was stirred at ambient temperature for 3 hours, during which time an additional portion of 4M hydrogen chloride in dioxane (8 ml, 24 mmol) was added. The mixture was evaporated to dryness and the residue dissolved in water (70 ml). This aqueous solution was added slowly to stirred 1M potassium carbonate solution (150 ml), causing a white solid to precipitate. The mixture was stirred for 10 minutes at ambient temperature. The precipitate was collected by filtration, washed with water and dried under vacuum to afford the title compound as a white solid (1.4 g, 89%) which was used without purification. ¹H NMR (500 MHz, DMSO, 27°C) δ 1.23 (6H, d), 2.98 (1H, hept), 4.90 (2H, s), 5.14 (2H, s), 6.50 (2H, d), 7.20 (2H, d), 7.82 (1H, s), 9.99 (1H, s); *m/z*: ES+ [M+H]⁺ 260.

2,6-Difluoro-4-(2-methoxyethoxy)benzotrile (12). 1-Bromo-2-methoxyethane (8.4 ml, 89 mmol) was added to a stirred suspension of 2,6-difluoro-4-hydroxybenzotrile (**11**) (11.5 g, 74.1 mmol) and potassium carbonate (30.7 g, 222.4 mmol) in DMF (175 ml). The mixture was heated to 85°C for 5 hours. The mixture was cooled to ambient temperature and was poured into water (1250 ml). The mixture was extracted with ethyl acetate (2 x 400 ml). The

1
2
3 combined extracts were washed with water (4 x 400 ml), saturated brine (200 ml), dried and
4
5 evaporated to dryness to give an orange oil. The crude product was purified by flash silica
6
7 chromatography, elution gradient 20 to 45% ethyl acetate in heptane. Pure fractions were
8
9 evaporated to dryness to afford the title compound as a white crystalline solid (16.1 g, 93%).
10
11 ¹H NMR (500 MHz, DMSO, 27°C) δ 3.28 (3H, s), 3.62 - 3.68 (2H, m), 4.21 - 4.27 (2H, m),
12
13 7.05 - 7.14 (2H, m); *m/z*: ES+ [M+H]⁺ 214.

14
15
16 **2-Amino-6-fluoro-4-(2-methoxyethoxy)benzonitrile (13).** 2,6-Difluoro-4-(2-
17
18 methoxyethoxy)benzonitrile (12) (23 g, 107.9 mmol) was split between 14 microwave vials,
19
20 each containing (1.64 g, 7.7 mmol) substrate. Each batch was suspended in isopropanol (3
21
22 ml) and concentrated aqueous ammonia solution (8 ml, 3237 mmol) was added. Each vial
23
24 was capped and heated to 100°C in microwave reactors for 13 hours. All batches were
25
26 combined; the solid which crystallised from solution was collected by filtration, washed with
27
28 water and dried to afford the title compound as a white crystalline solid (19.6 g, 87%). ¹H
29
30 NMR (500 MHz, DMSO, 27°C) δ 3.28 (3H, s), 3.57 - 3.64 (2H, m), 4.02 - 4.07 (2H, m), 6.10
31
32 (1H, dd), 6.17 (1H, dd), 6.35 (2H, s); *m/z*: ES- [M-H]⁻ 209.

33
34
35 **(*E*)-*N'*-(2-Cyano-3-fluoro-5-(2-methoxyethoxy)phenyl)-*N,N*-dimethylformimidamide**
36
37 **(14).** 1,1-Dimethoxy-*N,N*-dimethylmethanamine (62.6 ml, 471 mmol) was added to 2-amino-
38
39 6-fluoro-4-(2-methoxyethoxy)benzonitrile (11 g, 52.3 mmol) at 25°C. The resulting solution
40
41 was stirred at 80°C for 2 hours, then cooled to room temperature. The mixture was poured
42
43 into stirred water (200 ml) (exotherm, cold water cooling applied) and the reaction mixture
44
45 stirred for 1 hour. The mixture was extracted with ethyl acetate (2 x 150 ml). The combined
46
47 extracts were washed with water (3 x 150 ml), saturated brine (100 ml), dried and evaporated
48
49 to dryness to afford the title compound as a white crystalline solid (13.9 g, 100%). ¹H NMR
50
51 (500 MHz, DMSO, 27°C) δ 2.98 (3H, s), 3.07 (3H, s), 3.29 (3H, s), 3.61 - 3.66 (2H, m), 4.14
52
53 - 4.17 (2H, m), 6.55 - 6.6 (2H, m), 8.03 (1H, s); *m/z*: ES+ [M+H]⁺ 266.
54
55
56
57
58
59
60

***N*-(4-{{[5-Fluoro-7-(2-methoxyethoxy)quinazolin-4-yl]amino}phenyl)-2-[4-(propan-2-yl)-1*H*-1,2,3-triazol-1-yl]acetamide (44).** A mixture of *N*-(4-aminophenyl)-2-(4-isopropyl-1*H*-1,2,3-triazol-1-yl)acetamide (**10**) (5.4 g, 20.7 mmol) and (*E*)-*N'*-(2-cyano-3-fluoro-5-(2-methoxyethoxy)phenyl)-*N,N*-dimethylformimidamide (**14**) (5.2 g, 19.7 mmol) in acetic acid (12 ml) was stirred at 60°C for 35 minutes. The mixture was poured into water (150 ml), the mixture was stirred and sonicated. The resulting precipitate was collected by filtration, washed with water and dried. The solid was dissolved in DCM/methanol (12:1, 600 ml) and the solution washed with 0.2M NaHCO₃ solution (600 ml). The aqueous layer was extracted with DCM/methanol (12:1, 2 x 200 ml) and the extracts combined with the organic layer. The combined organic extracts were dried, filtered and evaporated to give a beige solid. The crude product was crystallised from hot ethanol (700 ml). After cooling to ambient temperature and stirring for 2 hours, the crystalline solid was collected by filtration, washed with cold ethanol and dried under high vacuum at 50°C to afford 7.4 g of crude product. The crude product was further purified by recrystallisation in hot ethanol (800 ml). After cooling to ambient temperature and stirring for 20 hours, the crystalline solid was collected by filtration; the solids were collected and dried under vacuum at 50°C for 72 hours to give the title compound as a white crystalline solid (6.2 g, 58%). ¹H NMR (500 MHz, DMSO) δ 1.27 (d, J = 6.9 Hz, 6H), 3.02 (heptd, J = 6.9, 0.6 Hz, 1H), 3.35 (s, 3H), 3.70 – 3.76 (m, 2H), 4.27 – 4.35 (m, 2H), 5.29 (s, 2H), 7.07 (d, J = 2.4 Hz, 1H), 7.15 (dd, J = 13.8, 2.4 Hz, 1H), 7.61 (d, J = 8.9 Hz, 2H), 7.69 (d, J = 8.9 Hz, 2H), 7.89 (d, J = 0.6 Hz, 1H), 8.47 (s, 1H), 8.98 (d, J = 9.7 Hz, 1H), 10.49 (s, 1H). ¹³C NMR (125 MHz, DMSO, 27°C) δ 22.5, 25.2, 52.1, 58.2, 68.0, 70.0, 99.8 (d, J = 11.5 Hz), 103.2 (d, J = 26.1 Hz), 104.6 (d, J = 3.2 Hz), 119.3, 122.1, 123.9, 134.3, 134.8, 152.8, 153.0, 155.6, 155.7 (d, J = 4.7 Hz), 158.5 (d, J = 253 Hz), 161.8 (d, J = 15.1 Hz), 164.2. *m/z* (ES⁺), [M+H]⁺ = 480; HRMS [MH]⁺ calcd for C₂₄H₂₇N₇O₃F: 480.2159; observed: 480.2178.

1
2
3
4
5 AUTHOR INFORMATION6
7 **Corresponding Author**8
9 *. Email: jason.kettle@astrazeneca.com
10
11
1213
14 ABBREVIATIONS USED
1516
17 ADME: absorption, distribution, metabolism, excretion. ATP: Adenosine triphosphate. GIST:
18 Gastrointestinal stromal tumors. PFS: Progression free survival. SEM: standard error of
19 means.
20
21
22
23
24
2526
27 **Associated Content**28
29 **Supporting Information Available** Protocols are provided for the cell assays and in vivo
30 experiments, synthetic methods for the remaining examples, together with crystallographic
31 information, and kinase panel selectivity data for compounds and molecular formula strings
32 with associated data. This material is available free of charge via the Internet at
33 <http://pubs.acs.org>. PDB depositions are available for compounds **18** (6GQJ and 6GQO), **23**
34 (6GQK and 6GQP), **35** (6GQL and 6GQQ) and **44** (6GQM). The authors will release the
35 atomic coordinates and experimental data upon article publication.
36
37
38
39
40
41
42
43
44
4546
47 ACKNOWLEDGMENTS
4849
50 We would like to thank Ian Hardern and Tina Howard for their help with protein production
51 and X-Ray crystallography respectively, together with Simon Woodcock, Lindsey Leach,
52 Martina Fitzek, Graham Sproat, Gareth Davies, Jarrod Walsh and Carolyn Blackett for
53
54
55
56
57
58
59
60

1
2
3 assistance with cell production, assay development and screening. We would also like to
4
5 thank Larry Bao for assistance in generating data to support pharmacodynamic assessment,
6
7 and Rodrigo Carbajo for key NMR characterisation.
8
9
10
11
12

13
14 ¹ Blay, J.-Y.; Casali, P.G.; Dei Tos, A.P.; Le Cesne, A.; Reichardt P. Management of gastrointestinal stromal
15 tumour: current practices and visions for the future. *Oncol.* **2015**, *89*, 1-13

16
17 ² Roberts, P. J.; Eisenberg, B. Clinical presentation of gastrointestinal stromal tumors and treatment of operable
18 disease. *Eur. J. Cancer* **2002**, *38*, S37–38

19
20
21 ³ Gatta, G.; van der Zwan, J. M.; Casali, P. G.; Siesling, S.; Dei Tos, A. P.; Kunkler, I.; Otter, R.; Licitra, L.;
22 Mallone, S.; Tavilla, A.; Trama, A.; Capocaccia, R. Rare cancers are not so rare: the rare cancer burden in
23 Europe. *Eur. J. Cancer* **2011**, *47*, 2493–2511

24
25
26 ⁴ Goettsch, W. G.; Bos, S. D.; Breekveldt-Postma, N.; Casparie, M.; Herings, R. M. C.; Hogendoorn, P. C. W.
27 Incidence of gastrointestinal stromal tumours is underestimated: results of a nation-wide study. *Eur. J. Cancer*
28 **2005**, *41*, 2868-2872

29
30
31 ⁵ Fletcher, J. A.; Rubin, B. P. KIT mutations in GIST. *Curr. Opin. Genet. Dev.* **2007**, *17*, 3–7

32
33
34 ⁶ Corless, C. L.; Schroeder, A.; Griffith, D.; Town, A.; McGreevey, L.; Harrell, P.; Shiraga, S.; Bainbridge, T.;
35 Morich, J.; Heinrich, M. C. PDGFRA mutations in gastrointestinal stromal tumors: frequency, spectrum and in
36 vitro sensitivity to imatinib. *J. Clin. Oncol.* **2005**, *23*, 5357-5364

37
38
39 ⁷ Din, O. S.; Woll, P. J. Treatment of gastrointestinal stromal tumor: focus on imatinib mesylate. *Ther. Clin.*
40 *Risk Manag.* **2008**, *4*, 149–162

41
42
43 ⁸ Zalcberg, J.; Verweij, J.; Casali, P.; Le Cesne, A.; Reichardt, P.; Blay, J. Y.; Schlemmer, M.; Van Glabbeke,
44 M.; Brown, M.; Judson, I. R. Outcome of patients with advanced gastro-intestinal stromal tumours crossing over
45 to a daily imatinib dose of 800mg after progression on 400mg. *Eur. J. Cancer.* **2005**, *41*, 1751-1757

46
47
48 ⁹ Mulet-Margalef, N.; Garcia-del-Muro, X. Sunitinib in the treatment of gastrointestinal stromal tumor: patient
49 selection and perspectives. *Onco. Targets Ther.* **2016**, *9*, 7573–7582

50
51
52 ¹⁰ Ferraro, D.; Zalcberg, J. Regorafenib in gastrointestinal stromal tumors: clinical evidence and place in
53 therapy. *Ther. Adv. Med. Oncol.* **2014**, *6*, 222–228
54
55
56
57
58
59
60

- 1
2
3
4 ¹¹ Chen, Y-Y.; Yeh, C-N.; Cheng, C-T.; Wu, C-E.; Chiang, K-C.; Chen, T-W.; Wang, C-C.; Chen, J-S.; Yeh, T-
5 S.; Fractioned dose regimen of sunitinib for patients with gastrointestinal stromal tumor: a pharmacokinetic and
6 treatment efficacy study. *Transl. Oncol.* **2014**, *7*, 620–625.
- 7
8
9 ¹² Grothey, A.; George, S.; van Cutsem, E.; Blay, J-Y.; Sobrero, A.; Demetrib, G. D.; Optimizing treatment
10 outcomes With regorafenib: personalized dosing and other strategies to support patient care. *Oncologist.* **2014**,
11 *19*, 669–680.
- 12
13
14 ¹³ Jung, F. H.; Morgentin, R. R.; Ple, P. Quinoline Derivatives. PCT Int. Appl. (2007), WO2007099323.
- 15
16 ¹⁴ Jung, F. H.; Ple, P. Quinazoline Derivatives. PCT Int. Appl. (2007), WO2007099317.
- 17
18 ¹⁵ Jung, F. H.; Ple, P. Quinoline Derivatives. PCT Int. Appl. (2007), WO2007099326.
- 19
20 ¹⁶ Jung, F. H.; Ple, P. Quinazoline Derivatives. PCT Int. Appl. (2006), WO2006040520.
- 21
22 ¹⁷ Martín, J.; Poveda, A.; Llombart-Bosch, A.; Ramos, R.; López-Guerrero, J.A.; García del Muro, J.; Maurel,
23 J., Calabuig, S.; Gutierrez, A.; González de Sande, J.L.; Martínez, J.; De Juan, A.; Lainez, N.; Losa, F.; Alija,
24 V.; Escudero, P.; Casado, A.; García, P.; Blanco, R.; Buesa, J.M.; Deletions affecting codons 557-558 of the c-
25 KIT gene indicate a poor prognosis in patients with completely resected gastrointestinal stromal tumors: a study
26 by the Spanish Group for Sarcoma Research (GEIS). *J. Clin. Oncol.* **2005**, *23*, 6190-6198.
- 27
28
29 ¹⁸ Wardelmann, E.; Losen, I.; Hans, V.; Neidt, I.; Speidel, N.; Bierhoff, E.; Heinicke, T.; Pietsch, T.; Büttner,
30 R.; Merkelbach-Bruse, S. Deletion of Trp-557 and Lys-558 in the juxtamembrane domain of the c-kit
31 protooncogene is associated with metastatic behavior of gastrointestinal stromal tumors. *Int. J. Cancer* **2003**
32 *106*, 887-895.
- 33
34
35 ¹⁹ Guo, T.; Agaram, N.P.; Wong, G.C.; Hom, G.; D'Adamo, D.; Maki, R.G.; Schwartz, G.K.; Veach, D.;
36 Clarkson, B.D.; Singer, S.; Dematteo, R.P.; Besmer, P.; Antonescu, C.R. Sorafenib inhibits the imatinib-
37 resistant KIT T670I gatekeeper mutation in gastrointestinal stromal tumor. *Clin. Cancer Res.* **2007**, *13*, 4874-
38 4881.
- 39
40
41 ²⁰ Garner, A.P.; Gozgit, J.M.; Anjum, R.; Vodala, S.; Schrock, A.; Zhou, T.; Serrano, C.; Eilers, G.; Zhu, M.;
42 Ketzer, J.; Wardwell, S.; Ning, Y.; Song, Y.; Kohlmann, A.; Wang, F.; Clackson, T.; Heinrich, M.C.; Fletcher,
43 J.A.; Bauer, S.; Rivera, V.M. Ponatinib inhibits polyclonal drug-resistant KIT oncoproteins and shows
44 therapeutic potential in heavily pretreated gastrointestinal stromal tumor (GIST) patients. *Clin. Cancer Res.*
45 **2014**, *20*, 5745-5755.
- 46
47
48
49
50
51
52
53
54
55
56
57
58
59
60

- 1
2
3
4 ²¹ Aleksandrov, A.; Simonson, T.; Molecular dynamics simulations show that conformational selection governs
5 the binding preferences of imatinib for several tyrosine kinases. *J. Biol. Chem.* **2010**, *285*, 13807-13815.
6
7 ²² DiNitto, J. P.; Deshmukh, G. D.; Zhang, Y.; Jacques, S. L.; Coli, R.; Worrall, J. W.; Diehl, W.; English, J. M.;
8 Wu, J. C. Function of activation loop tyrosine phosphorylation in the mechanism of c-Kit auto-activation and its
9 implication in sunitinib resistance. *J. Biochem.* **2010**, *147*, 601-609.
10
11 ²³ Rose, S. BLU-285, DCC-2618 show activity against GIST. *Cancer Discov.* **2017**, *7*, 121-122.
12
13 ²⁴ Janku, F.; Razak, A. R. A.; Gordon, M. S.; Brooks, D. G.; Flynn, D. L.; Kaufman, M.; Pitman, J.; Smith, B.
14 D.; Somaiah, N.; De Groot, J. F.; Chen, G.; Jennings, J.; Salah, S.; Westwood, D.; Gerstenberger, E.; Rosen, O.;
15 George, S. Pharmacokinetic-driven phase I study of DCC-2618 a pan-KIT and PDGFR inhibitor in patients (pts)
16 with gastrointestinal stromal tumor (GIST) and other solid tumors. *J. Clin. Oncol.* **2017**, *35* (suppl; abstr 2515).
17
18 ²⁵ Evans, E.; Gardino, A.; Hodous, B.; Davis, A.; Zhu, J.; Kohl, N. E.; Lengauer, C. Blu-285, a potent and
19 selective inhibitor for hematologic malignancies with KIT exon 17 mutations. *Blood* **2015**, *126*, 568.
20
21 ²⁶ Plé, P. A.; Jung, F.; Ashton, S.; Hennequin, L.; Laine, R.; Morgentin, R.; Pasquet, G.; Taylor, S. Discovery of
22 AZD2932, a new quinazoline ether inhibitor with high affinity for VEGFR-2 and PDGFR tyrosine kinases.
23 *Bioorg. Med. Chem. Lett.* **2012**, *22*, 262–266.
24
25 ²⁷ Plé, P. A.; Jung, F.; Ashton, S.; Hennequin, L.; Laine, R.; Lambert-van der Brempt, C.; Morgentin, R.;
26 Pasquet, G.; Taylor, S. Discovery of new quinoline ether inhibitors with high affinity and selectivity for PDGFR
27 tyrosine kinases. *Bioorg. Med. Chem. Lett.* **2012**, *22*, 3050–3055.
28
29 ²⁸ Goldberg, F. W.; Kettle, J. G.; Kogej, T.; Perry, M. W. D.; Tomkinson, N. P. Designing novel building blocks
30 is an overlooked strategy to improve compound quality. *Drug Discov. Today* **2015**, *20*, 11-17.
31
32 ²⁹ Beglov, D.; Roux, B. An integral equation to describe the solvation of polar molecules in liquid water. *J.*
33 *Phys. Chem. B*, **1997**, *101*, 7821–7826.
34
35 ³⁰ Kettle, J. G.; Wilson, D. M. Standing on the shoulders of giants: a retrospective analysis of kinase drug
36 discovery at AstraZeneca. *Drug Discov. Today* **2016**, *21*, Pages 1596-1608.
37
38 ³¹ Bergenholm, L.; Parkinson, J.; Mettetal, J.; Evans, N. D.; Chappell, M. J.; Collins, T. Predicting QRS and PR
39 interval prolongations in humans using nonclinical data. *Br. J. Pharmacol.* **2017**, *174*, 3268-3283.
40
41
42
43
44
45
46
47
48
49
50
51
52
53
54
55
56
57
58
59
60

